Nuclear Engineering and Design 239 (2009) 455–469

Contents lists available at ScienceDirect

Nuclear Engineering and Design

journal homepage: www.elsevier.com/locate/nucengdes

A case study of the effect of cladding panels on the response of reinforced concrete frames subjected to distant blast loadings

Bing Li*, Tso-Chien Pan, Anand Nair

Protective Technology Research Center, Nanyang Technological University, 50 Nanyang Ave, Singapore 639798, Singapore

ARTICLE INFO

Article history:
Received 6 September 2008
Received in revised form 1 December 2008
Accepted 1 December 2008

ABSTRACT

The turbine building is a vital structure within nuclear power plants that houses turbines, moisture separators and electric generators among other important equipment. Turbine buildings are typically frame structures that in most cases have not been designed to resist blast loadings. The authors to determine the dynamic responses of reinforced concrete (RC) frame structures when subjected to distant intense surface loadings caused by explosions carried out a numerical study. The study was extended further to investigate the influence of claddings on frame structures when exposed to blast loadings. A three-dimensional (3D) nonlinear dynamic finite element model was created and utilized to determine the dynamic responses of RC frame structures from both local and global perspectives. It was observed from the results obtained from the finite element (FE) simulations carried out that the dynamic responses of frame structures with claddings were more severe. This is due to the variations in blast forces received by the structure.

1. Introduction and background

Security in nuclear power plants has to take an additional heightened level with the recent surge in the occurrence of worldwide explosive events caused by terrorism. In nuclear power plants, boiling water reactors present unique challenges since the water going through the turbines are radioactive. This means that the turbine hall has to be slightly contained and may require unique maintenance routines. The focus of this study is to investigate the behavior of these turbine buildings, which are typically frame structures, when subjected to distant blast loadings.

After the trigger of a blast, a blast wave including a high-pressure shock front is formed and expands outward from the center of detonation (ASCE, 1985; Biggs, 1964; Baker et al., 1983; Forbes, 1999; Smith and Hetherington, 1994). As the blast wave strikes a building, explosive detonations may cause extensive damage to both the target structure and nearby buildings. The analysis of overpressure and drag force of the blast wave load on a structure, and the interaction between them is extremely complicated. However, considering the relative distance of the detonation center with the target structure as well as the size of the structure itself, two classes of blast wave-structure interaction can be generally identified and is shown in Fig. 1 (Smith and Hetherington, 1994). The first class is the interaction of a blast wave produced by the detonation of a smaller charge loading a target structure at a short standoff distance, which is typical for most terrorist attacks such as car bombings (Corley et al., 1998; Longinow and Mniszewski, 1996; Luccioni et al., 2003). The second class is the interaction of a blast wave on a relatively distant structure as might be present due to an accidental severe surface explosion of petroleum refineries, chemical plants, ammunition storage areas (Glasstone and Dolan, 1977; Kletz, 1975) and turbine buildings.

The profile of blast loadings on a structure tends to be different within these two classes of blast wave-structure interaction. In the first class, the blast pressures are produced locally to individual structural members and the members are likely to be loaded sequentially. In contrast, during the second class of blast wave-structure interaction, the target structure is engulfed due to the diffraction of the blast wave and a normal squashing force will be applied to all of the exposed surfaces. There is also a translational drag force, which tends to move the body of the structure laterally. Many explosion tests and numerical analyses have been carried out to determine the behaviors of structures in the first class of blast wave-structure interaction where the blast pressures are applied locally to individual structural members. This results in the possibility of an excessive local failure of several critical structural members that could lead to a progressive collapse noticeably in a non-redundant structure (Corley et al., 1998; Longinow and Mniszewski, 1996; Luccioni et al., 2003). However, little literature is available due to the limited research that has been devoted towards the behavior of structures and their possible failure mechanisms in the second class of blast wave-structure interaction.

* Corresponding author.
E-mail address: cbli@ntu.edu.sg (B. Li).

0029-5493/$ – see front matter © 2008 Elsevier B.V. All rights reserved.
doi:10.1016/j.nucengdes.2008.12.003

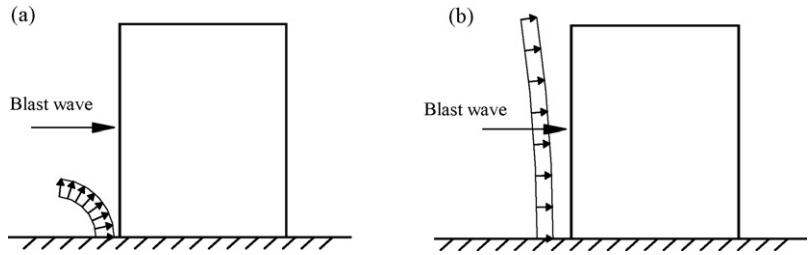

Fig. 1. Two classes of blast wave-structure interaction.

The blast incidents producing the second class of blast wave-structure interaction are very rare. If they do occur, the consequence can be extremely severe, particularly upon structures not specifically designed to withstand blast effects. There have been cases of severe damage or even collapse of surrounding buildings caused by the event of such incidents (Glasstone and Dolan, 1977; Kletz, 1975). This would be a very catastrophic event in a nuclear power plant. To minimize blast consequences to buildings, an effective blast resistant design is needed. For this purpose, knowledge of structural dynamic behaviors and the corresponding potential damage distributions under such blast situations is imperative. This paper presents a case study of the structural behaviors in the second class of blast wave-structure interaction. The study is focused on moment-resisting RC frame structures, which is the typical design adopted in turbine buildings. The results emphasizes on the complicated interaction between the blast wave, and structure as well as the nonlinear material properties of concrete and reinforcement. Since the exterior cladding panels might have noticeable effects on the structural behaviors under blast conditions, two types of multi-storey frame structures, with and without exterior cladding panels are analyzed. The corresponding structural dynamic responses are identified and compared. The findings from this study are used to reach conclusions and recommendations in the blast resistant design concerning explosive safety for typical turbine buildings in nuclear power plants.

2. Blast loadings

The hemispherical wave front, produced by distant intense surface explosions that, exerts loading on the frame structure by subjecting it to blast waves produced by distant intense surface explosions, can be reasonably idealized as a planar blast wave front. The idealization is conducted by considering the size of the face of the structure that is essentially parallel to the front faces of the target as illustrated in Fig. 2. As the blast wave strikes on the front face of a closed structure target, a reflected pressure is instantly developed. The blast wave diffracts around the target, subjecting initially the sides and roof and finally the rear face to pressures equal to incident overpressures (air-blast pressure occurring in the free-field). At the same time, these faces are loaded by drag pressures that are a function of a drag coefficient. This dynamic pressure is associated with the airflow behind the shock causing drag or wind type loads. The pressure causes a push on the front face of the target followed by a suction force on the back and sides as the blast dynamic pressure passes over and around the target (Forbes, 1999; Smith and Hetherington, 1994).

Determination of the exact blast loadings created by a distant explosion on the front, top sides, and the rear faces of the closed target is almost unrealistic considering the complicated process of the interaction of the blast wave with the target in concern. In order to reduce this complex problem of blast loadings to reasonable terms,

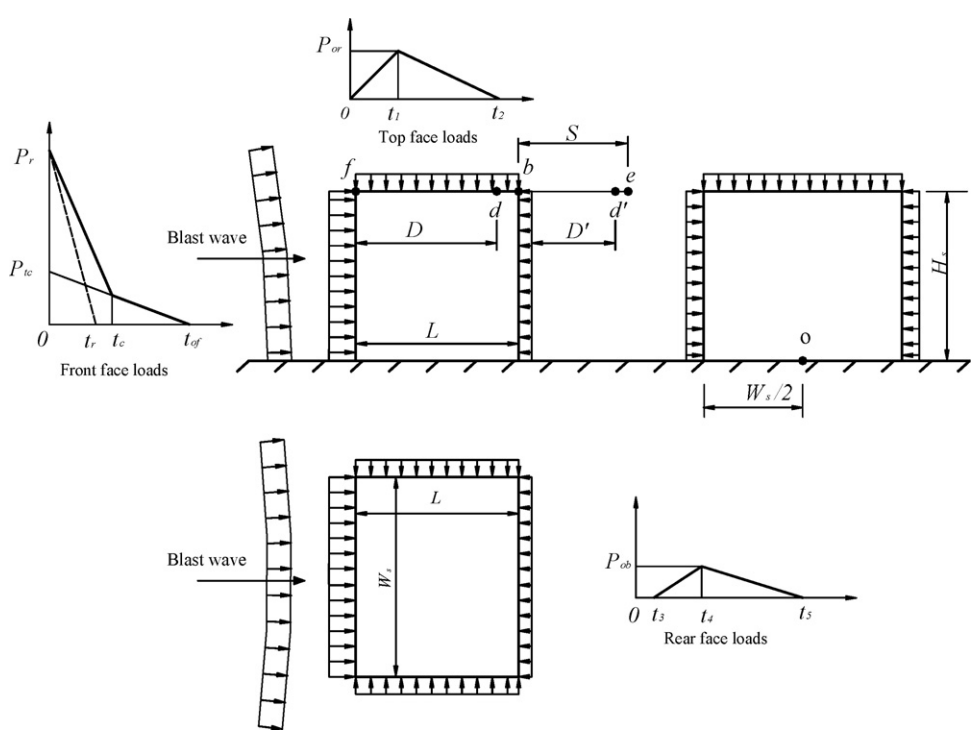

Fig. 2. Blast loadings on a simply closed rectangular target.

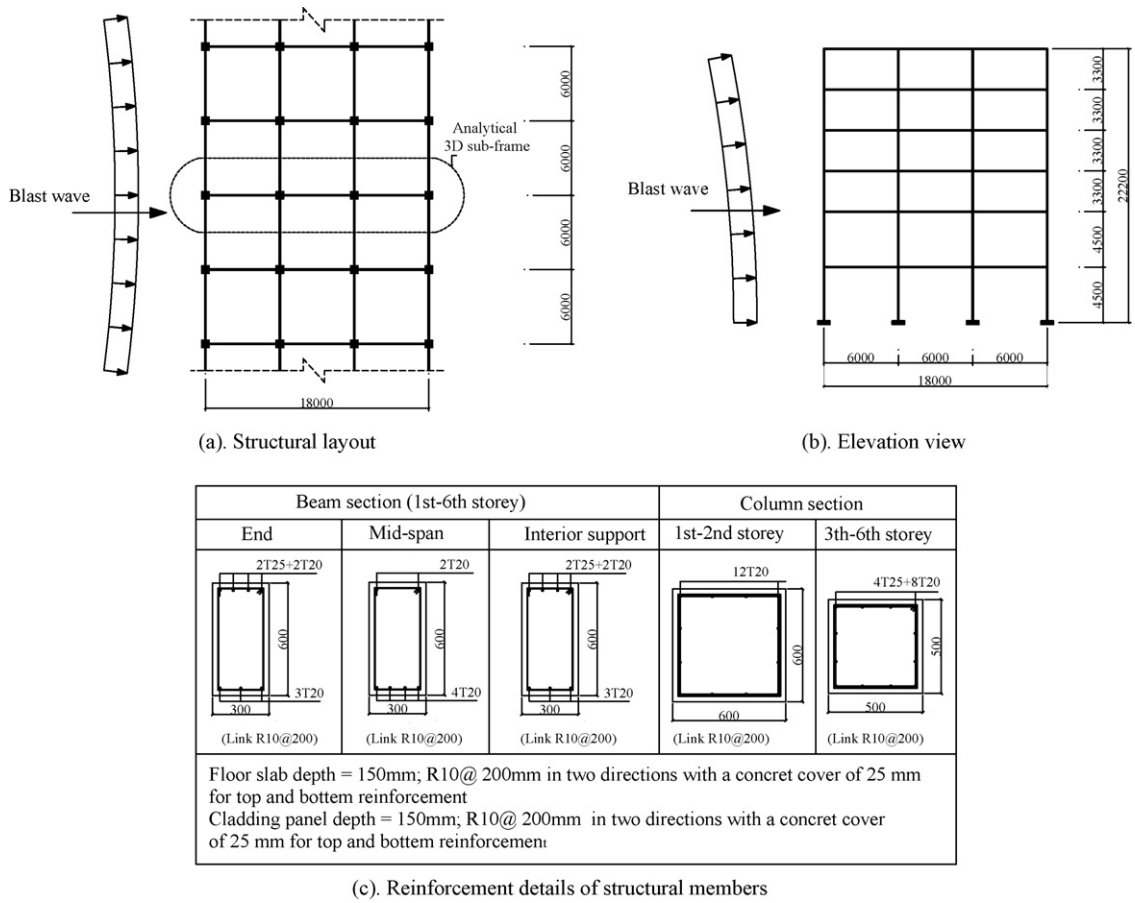

Fig. 3. Details of the target six-storey frame structure. (a) Structural layout. (b) Elevation view. (c) Reinforcement details of structural members.

a computational procedure is recommended in TM 5-855-1 (1986) based on two assumptions that (a) the target is generally rectangular in shape, and (b) the object being loaded is in the region of the Mach reflection (ASCE, 1985; TM 5-855-1, 1986). These two assumptions are computed in a rational manner during the derivation of the blast loadings on rectangular targets in a relatively large standoff blast environment. The simplified loading configurations on various faces are shown in Fig. 2 whose parameters can be calculated with the equations listed in TM 5-855-1 (1986) for a closed rectangular aboveground target, i.e. a column, a beam, or a closed structure.

The computation of the blast loadings on a frame structure is relatively more complicated than illustrated in Fig. 2. This is caused by the fact that the frame structure as a whole not being able to be taken as an arbitrarily closed rectangular target. The loading profiles applied to a frame structure are dependent on the out-of-plane strength and stiffness of exterior cladding panels, as well as their connection details within the beam and column members

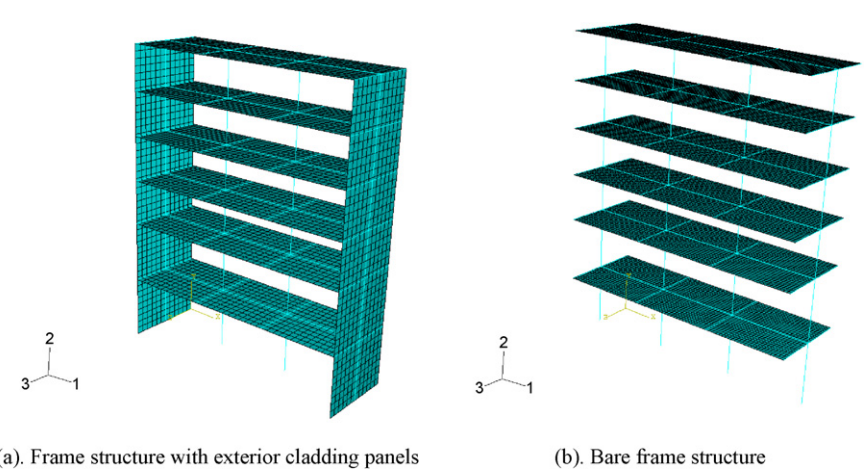

Fig. 4. Modeling of the three-dimensional six-storey sub-frame structure. (a) Frame structure with exterior cladding panels. (b) Bare frame structure.

that make up the frame when subjected to the direct action of blast loadings. In this study, two extreme cases are considered:

- exterior cladding panels constructed from reinforced concrete that posses significant strength and stiffness;
- no exterior cladding panels for the frame structure (bare frame structure).

For the case of the frame structure with exterior cladding panels made out of RC, the cladding panels possess significant out-of-plane strength, stiffness and strong connection details with other frame members. As the blast wave hits the outer surfaces of the structure (including outer surfaces of exterior cladding panels, exterior beams and columns), it would not be able to penetrate into the structure. The blast loadings subjected to the cladding panels would in turn be transferred to its primary frame members through reaction forces. These transferred reaction forces together with the blast loadings acting directly on the outer surfaces of the exterior beams and columns will produce a dynamic response from the structure. The method utilized to compute the blast forces exerted upon the front, roof and rear surfaces of the structure adopts this methodology and assumes that it is reasonable to treat the whole structure as a closed target.

In the second case, the blast wave front would enter the building producing a high pressure on the rear faces of the columns. This varied load path implies that the structure as a whole cannot be assumed to take the form of a closed rectangular target. This means the pressure distribution illustrated in Fig. 2 cannot be used directly as when computing blast loadings on a bare frame structures. However, the shock wave front from a distant surface explosion condition is essentially parallel to the front faces of the blast-loaded columns and thus, the blast loading subjected to individual columns of the structure can be computed by taking each of its front faced columns as a closed rectangular target. The blast forces on the front and rear faces of the columns can then be evaluated in accordance to Fig. 2. The parameters (L, W_s and H_s) are equal to those of the dimensions of each individual column. The blast loadings on both side faces of each column are identical. This causes the top and bottom surfaces of each slab to have identical loadings which in turn leads to it experiencing a zero resultant force due to the blast wave. This loading thus approximates to one produced by a planar wave, and therefore is not accounted for during the analysis.

In addition to the effects of blast overpressures, intense surface explosions are also capable of producing ground shocks as a result of the directly induced ground motion propagating through the soil or rock and might have some effect on structural responses. The arrival time of these ground shocks would differ from the arrival time of the blast wave on the structure. However, considering the fact that the target to be studied is located at a large standoff distance relative to the source of explosion, the magnitude of the ground shock would have been greatly diminished. Therefore the effects of direct ground shocks are ignored in this analysis.

3. Design of the target frame structure

A three-dimensional, six-storey moment-resisting RC frame structure is designed in accordance with the design code BS 8110 (1997) to study the dynamic behaviors of frame structures under the distant blast conditions. The layout of the structure and the reinforcement details within structural members are shown in Fig. 3.

The blast wave produced by detonating the equivalent weight of 50 tons of TNT placed at ground level at a standoff distance of 100 m is considered in this study. In these blast conditions, where the standoff distance is significantly larger than the size of the target structure, the blast wave can be reasonably modeled as a planar wave as illustrated in Fig. 3. This planar wave engulfs the whole structure resulting in uniformly distributed blast pressures on all its exposed surfaces along both the width and height of the target. Due to the symmetry in both the configuration of the target structure and the blast pressure distribution, a three-dimensional sub-frame including a planar frame and half of its adjacent components are modeled to simulate the dynamic responses of the whole structure.

Two separate numerical simulations are performed on the six-storey frame structure in order to determine the effect of the exterior cladding panels on the structural blast responses. In the first model, the exterior cladding panels are assumed to be made of RC with sufficiently out-of-plane strength and stiffness to prevent the blast waves from entering the building. This model includes exterior cladding panels (whose reinforcement arrangements are found in Fig. 3c), together with the floor slabs, beams and columns. In the second model, the structure is built without exterior cladding panels. As discussed previously, such a frame structure can be assumed as a bare frame against the blast loadings. Accordingly, only beams, columns and floor slabs are modeled for the numerical simulations in the second model. The modeling of frames for these models is illustrated in Fig. 4.

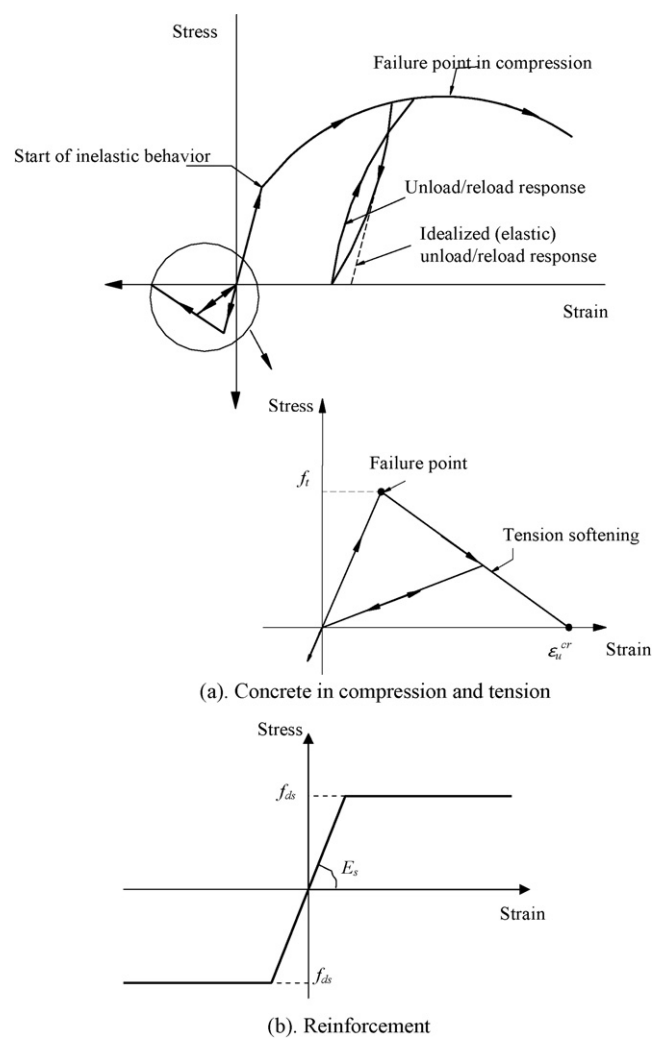

Fig. 5. Material modeling. (a) Concrete in compression and tension. (b) Reinforcement.

4. Finite element models

The three-dimensional six-storey sub-frame structures are modeled to perform the numerical simulations of the structural dynamic responses under the concerned blast conditions by utilizing the ABAQUS (2005) computer software. The finite element modeling process consists of structural modeling, material modeling of concrete and reinforcement, type of loads, analysis steps, and the integration methods.

4.1. Structural modeling

Two types of structural members are included in the sub-frames. They include beams and columns and the planar members that comprise of exterior cladding panels and floor slabs. In order to obtain a more accurate simulation of the structural response when subjected to blast conditions, three-dimensional continuum solid elements were employed when modeling these structural members. However, creation of these elements demands considerably greater computational effort due to the complicated nonlinear behaviors of the materials and results in an extremely large size of the finite element model. For simplicity, Timoshenko beam elements for modeling frame beams and columns, together with 4-node shell elements for exterior cladding panels and floor slabs were adopted. The accuracy of the numerical simulation results of the responses for different structural members modeled as the beam or shear elements will be examined by comparison with the available data in the latter part of this paper. Reinforcements within the concrete structures are modeled by means of rebars, which are one-dimensional strain theory elements (rods) defined singly or embedded in oriented surfaces. Each rebar is placed at its corresponding location for the beam elements while the layers of rebar are defined using the shell elements with the needed data-input of reinforcing bar's area and location, and its space length. The structural modeling for the six-storey frame structure with/without exterior cladding panels is shown in Fig. 4. The bottom ends of structural columns are modeled to be perfectly fixed to the solid ground and symmetry boundary conditions are applied to the edges of the slabs and cladding panels.

4.2. Material modeling

The dynamic responses of RC structures under blast conditions are highly dependent on the material properties of the concrete and reinforcement that each of its individual members is made up from. The accurate modeling of the material properties is essential to ensure the validity in the results from the numerical simulations that determine the dynamic responses of structures. In finite element analysis, the material behaviors of concrete, reinforcing bars and the bond between them should be taken into account. It is presumed that the bars form a perfect bond with concrete. Although this assumption will impose a certain level of errors, it is the only practical means of finding a solution for the numerical simulations to determine the responses of RC structural systems. This is caused by the unmanageable size of the computational works and the lack of reliable data on the topic of blast environments.

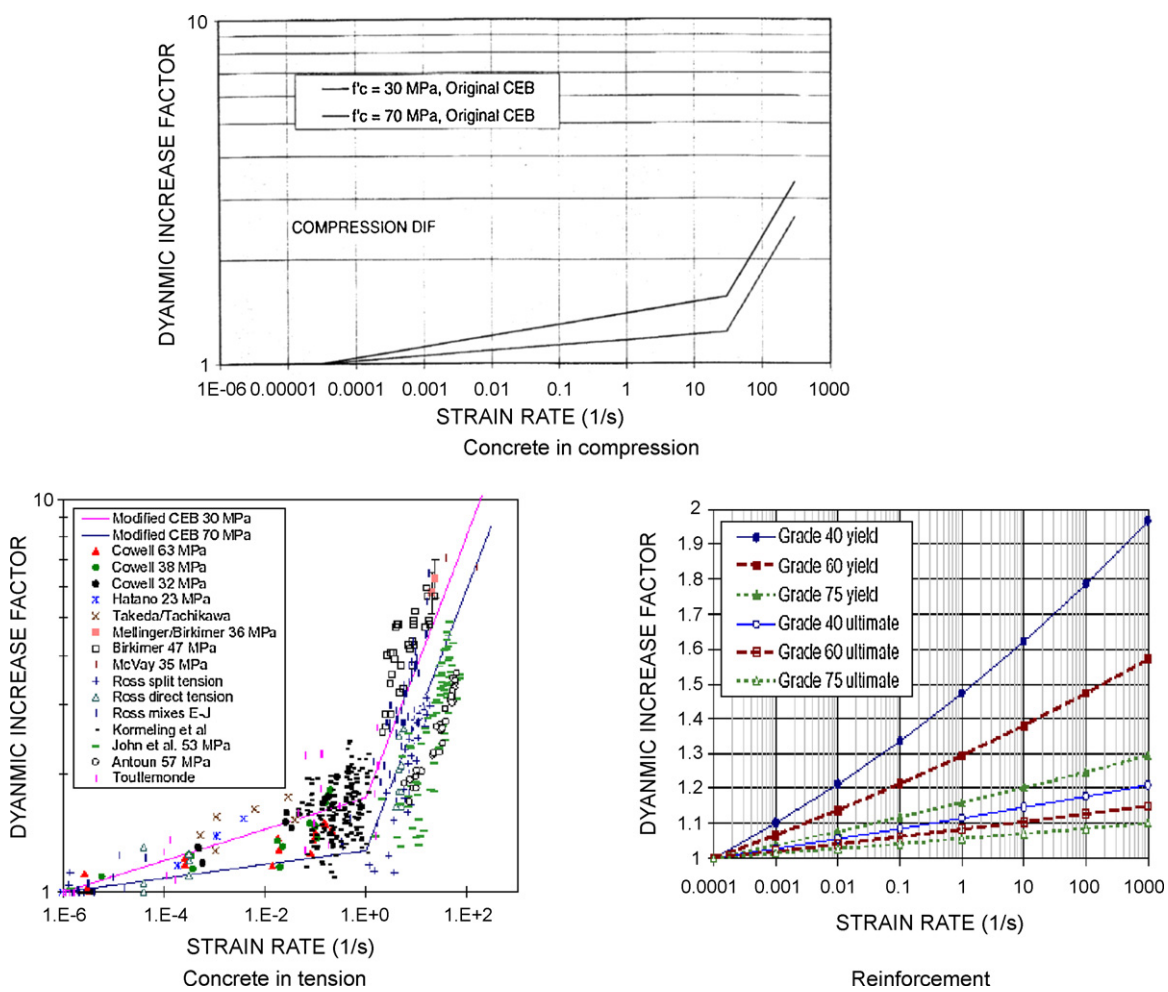

Fig. 6. DIFs for concrete and reinforcement.

The smeared cracking model is utilized to represent the tensile behavior of concrete. In this model, concrete begins to crack as the surface reaches the defined maximum principal tensile stresses. This will in turn affect the stress and material stiffness associated with each material point at the related elements. To simulate the softening effect of the concrete in tension after cracking, a bilinear tension stress–strain curve is defined as in Fig. 5, where ε_u^{cr} is taken as 10^{-3}. The selection of this value is based on the assumption that the strain softening after failure reduces the stress linearly to zero at a total strain of about 10 times the strain at failure of concrete in tension, which is typically 10^{-4} in standard concrete (Hilleborg et al., 1976). The tensile strength f_t is determined from the compressive strength f_c as (CEB-FIP, 1993)

$$f_t = 0.30 f_c^{2/3} \tag{1}$$

In compression, concrete is simulated by an elastic–plastic model where the elastic stress state is limited by a yield surface. Once yielding has occurred, an associated flow rule with isotropic hardening is used. This yield surface can be written in terms of the first two stress invariants as

$$f = q - \sqrt{3}a_0 p - \sqrt{3}\sigma_c(\varepsilon_{uniaxial}^{pl}) \tag{2}$$

where p is the effective pressure, q is Mises equivalent deviatoric stress, and a_0 is a constant, which is chosen from the ratio of the ultimate stress reached in biaxial compression to the ultimate stress reached in uniaxial compression. $\sigma_c(\varepsilon_{uniaxial}^{pl})$ is the hardening (and softening) parameter, which is defined from the uniaxial compression data of the concrete as a function of its plastic strain. The stiffness used in the analysis for unloaded concrete in tension and compression is given in Fig. 5. When the cracked concrete is unloaded, the secant unloading modulus is utilized as stiffness so that the strain across the crack is reduced linearly to zero as the stress approaches zero. If the load is removed at some point after inelastic straining has occurred for the concrete in compression, the unloading response would be softer than the initial elastic response, but this effect is ignored in this model. Thus initial elastic stiffness is used when the concrete in compression is unloaded.

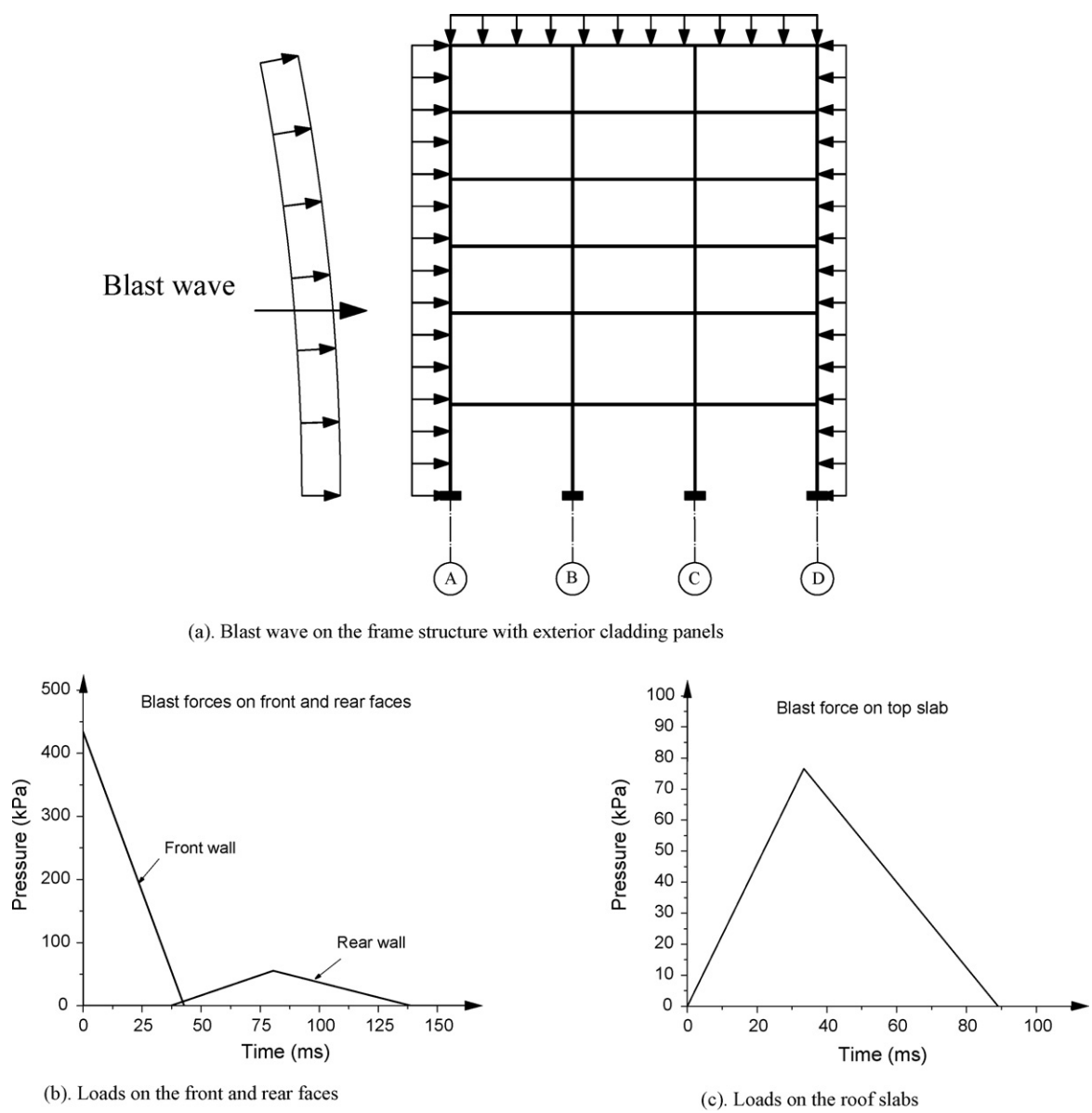

Fig. 7. Blast loadings on the frame structure with exterior cladding panels. (a) Blast wave on the frame structure with exterior cladding panels. (b) Loads on the front and rear faces. (c) Loads on the roof slabs.

The Von-Mises yield criterion is used to describe the constitutive behavior of the reinforcement within the concrete. The stress–strain relationship of reinforcement is shown in Fig. 5, where the reinforcement is modeled as an elasto-plastic curve. Strain hardening of reinforcement is not considered in this analysis due to the lack of experimental data available to support it. The ultimate strain value is often not reported in current literatures because of the difficulty in determining the exact peak stress when it occurs

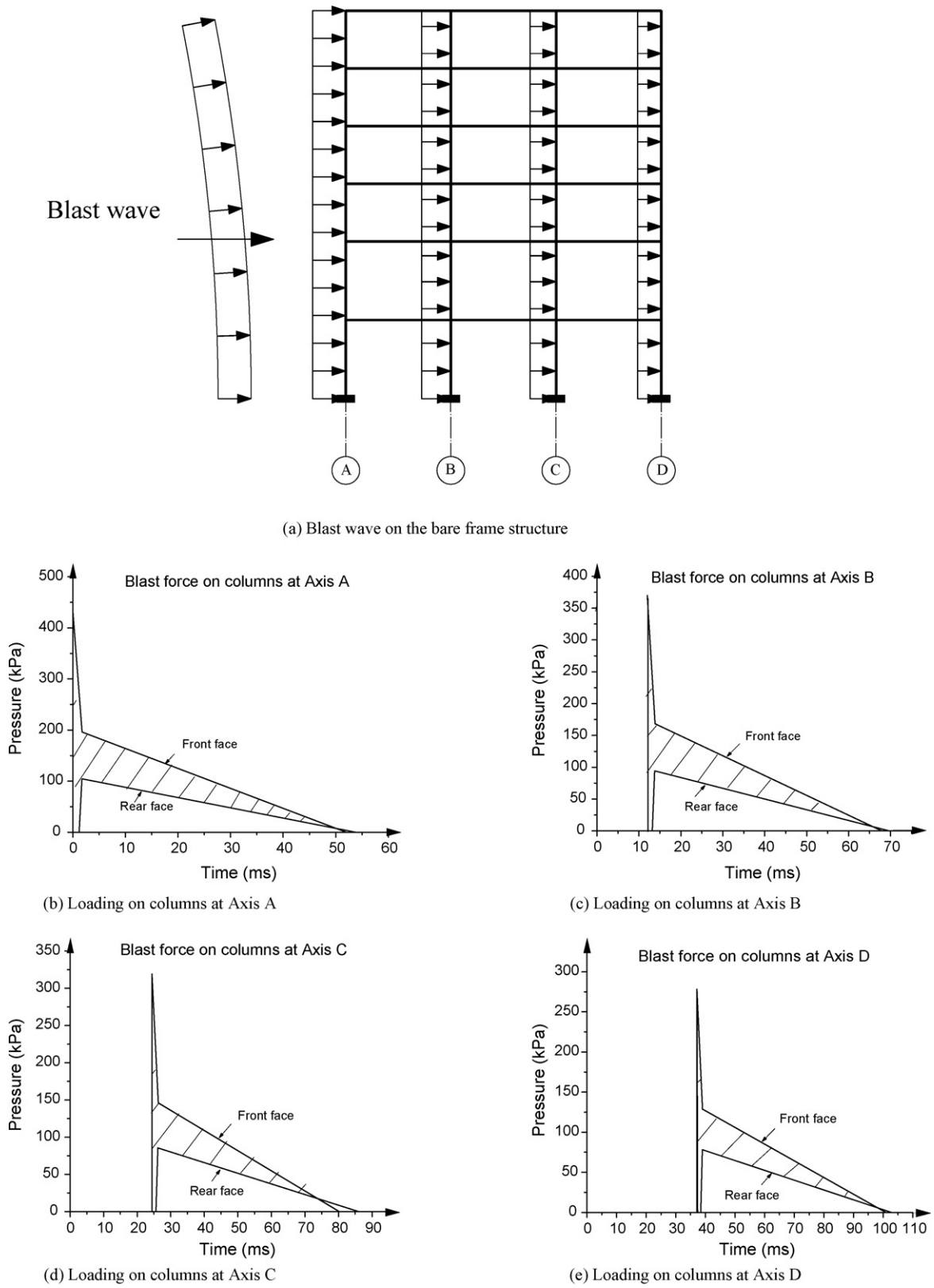

Fig. 8. Blast loadings on the bare frame structure. (a) Blast wave on the bare frame structure. (b) Loading on columns at Axis A. (c) Loading on columns at Axis B. (d) Loading on columns at Axis C. (e) Loading on columns at Axis D.

and also because of the unresolved ability to distinguish between the materials ultimate and its rupture strain.

In order to consider the fact that under higher loading rates in both concrete and reinforcement exhibit increased strengths (Dharan and Hauser, 1970; Fu et al., 1991; Georgin et al., 1998; Malvar and Crawford, 1998a,b), a dynamic increase factor (DIF), defined as the ratio of the dynamic to static strength, is employed in this analysis. The expressions by Malvar and Crawford (1998a,b) are utilized and are derived from a literature review comprising of extensive test data revealing the effects of strain rate on the strength of concrete and reinforcement. For the concrete compressive strength, DIF is given as

$$DIF = \begin{cases} (\dot{\varepsilon}/\dot{\varepsilon}_s)^{1.026\alpha_s} & \dot{\varepsilon} \le 30\ \mathrm{s}^{-1} \\ \gamma_s(\dot{\varepsilon}/\dot{\varepsilon}_s)^{1/3} & \dot{\varepsilon} > 30\ \mathrm{s}^{-1} \end{cases} \tag{3}$$

where $\dot{\varepsilon}$ is the strain rate in the range of 30×10^{-6} to $300\,\mathrm{s}^{-1}$; $\dot{\varepsilon}_s = 30 \times 10^{-6}\ \mathrm{s}^{-1}$ (static strain rate); $\log \gamma_s = 6.156\alpha_s - 2$; $\alpha_s = 1/(5 + 9f_c/f_{co})$; $f_{co} = 10\,\mathrm{MPa}$; f_c is the static compressive strength of concrete. For the concrete in tension, the formula is

$$DIF = \begin{cases} (\dot{\varepsilon}/\dot{\varepsilon}_s)^{\delta} & \dot{\varepsilon} \le 1.0\,\mathrm{s}^{-1} \\ \beta(\dot{\varepsilon}/\dot{\varepsilon}_s)^{1/3} & \dot{\varepsilon} > 30\,\mathrm{s}^{-1} \end{cases} \tag{4}$$

where $\dot{\varepsilon}$ is the strain rate in the range of 10^{-6} to $160\,\mathrm{s}^{-1}$; $\dot{\varepsilon}_s = 10^{-6}\,\mathrm{s}^{-1}$; $\log \beta = 6\delta - 2$; $\delta = 1/(1 + 8f_c/f_{co})$; $f_{co} = 10\,\mathrm{MPa}$. A plot of the proposed formulae for the *DIF* of concrete in tension and compression is shown in Fig. 6, which indicates that the strength enhancement is different for tension and compression. The *DIF* formula for the yield stress of reinforcement (Malvar and Crawford,

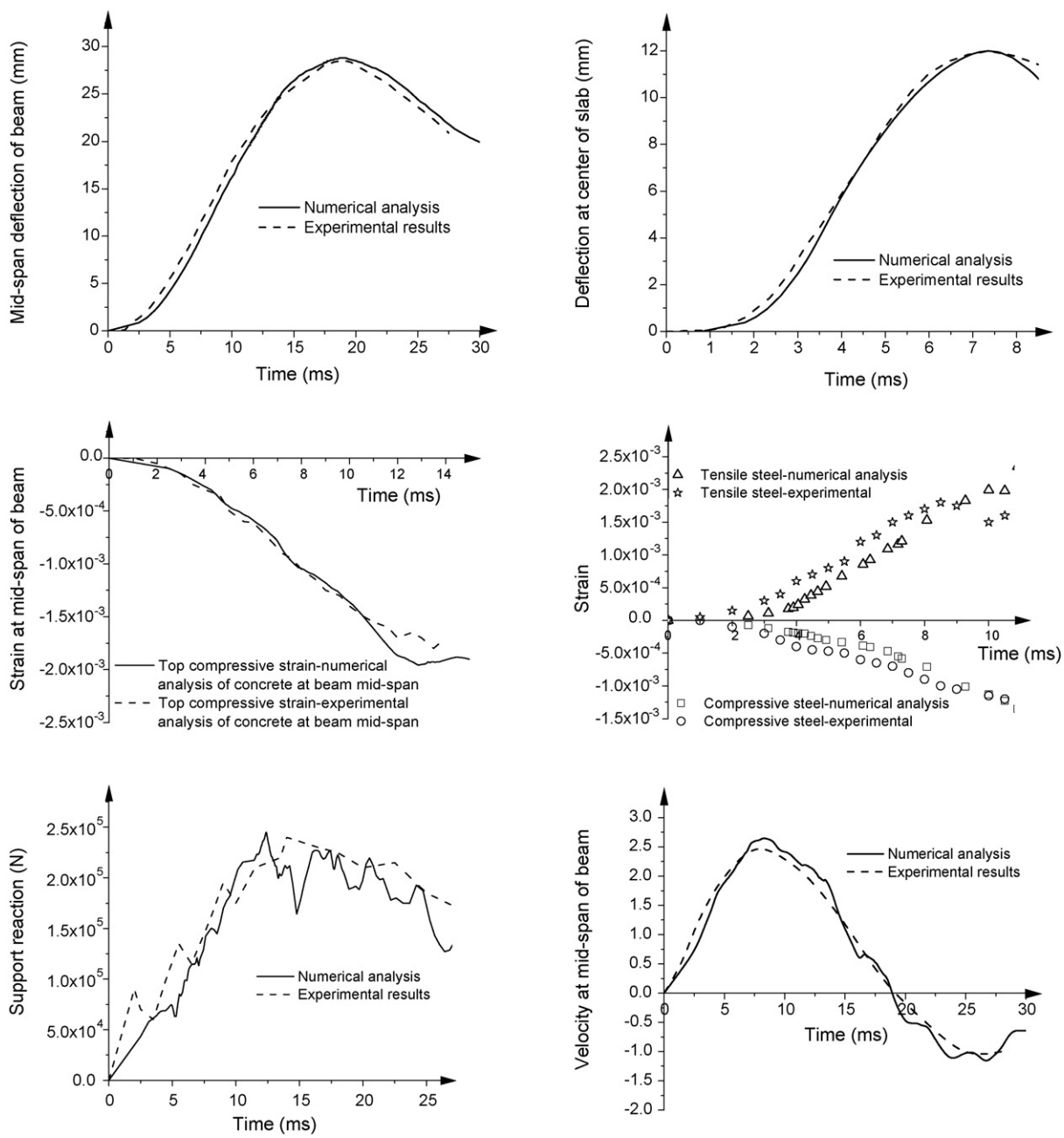

Fig. 9. Verification of finite element models showing comparison between the numerical and experimental results.

1998a,b) is

$$DIF = \left(\frac{\dot{\varepsilon}}{10^{-4}}\right)^{\alpha} \quad (5)$$

where $\alpha = \alpha_{fs}$ and $\alpha_{fs} = 0.074 - 0.04\, f_s/414$; f_s is the reinforcement static yield strength in MPa. This formula is valid for reinforcement with yield stresses between 290 and 710 MPa and for strain rates between 10^{-4} and 225 s^{-1}.

The user subroutine USDFLD in ABAQUS is used to integrate Eqs. (3)–(5) into the analysis. This subroutine allows the user to define the field variable of a material point as a function of any of the available material point quantities. Thus by taking the strain rate as a field variable, the strain rate-dependent material properties can be introduced into the analysis since such properties can be easily defined as functions of the strain rate with Eqs. (3)–(5).

4.3. Application of loads and analysis procedure

Two steps of analyses are carried out in accordance to two different loading stages, during the simulation to determine the structural blast responses. The service loads would initially be imposed onto the structure prior to the occurrence of the explosion. The intensity and distribution of the stresses and strains induced by the service loads will influence the structural behaviors when subjected to blast conditions. Thus nonlinear static analysis is performed prior to the three-dimensional sub-frame structure being subjected to the service loads. The loads included in this step are the live loads, the dead loads and the super imposed dead loads. The second step is to determine the dynamic response simulation of frame structures when loaded by the blast wave pressures. Nonlinear dynamic analysis is performed at this stage. The functions of the blast pressures subjected to the structures that are necessary in this step for both the bare frame and for the frame with exterior cladding panels are discussed in the following subsection.

For the frame structure with RC exterior cladding panels, the blast force functions applied on the front, top and rear surfaces are evaluated by taking the whole structure as a closed rectangular target and are illustrated in Fig. 7. In this case, the reflected pressure dominates the blast loadings on the front cladding panels. As for the top and rear surfaces, the dominating blast pressures are composed of the incident overpressure and dynamic pressure.

In contrast, the planar wave enters the structure loading each of the exposed columns, of the bare frame structure. This imposes the blast loading on each column by taking it as a closed rectangular target. The functions of blast forces on each of its front and rear faces are obtained and the results under this blast condition are shown in Fig. 8. The shaded area represents the net blast pressure on each column. It is demonstrated that due to the relatively small dimension of the column width, the reflected pressure decays rapidly and the drag force correlated with dynamic pressure plays a vital role in the net blast loadings subjected on to the columns. The peak pressure lessens while the lag time rises up as the distance between the blast source and the target gets further apart. Comparisons between Figs. 7 and 8 indicate that there are obvious differences in the spatial distribution as well as the time history for the blast loadings acting on the structures between the two cases.

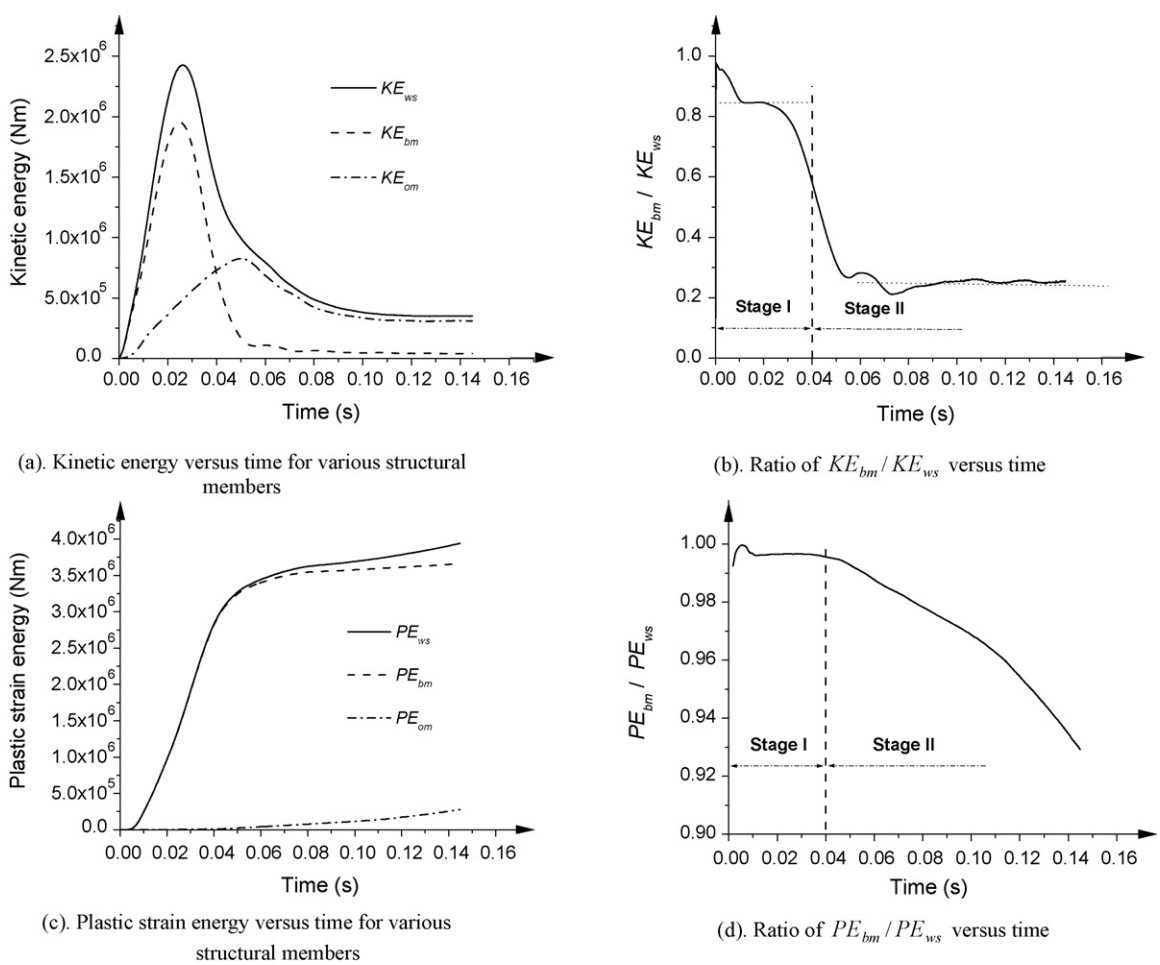

Fig. 10. Response of kinetic energy and plastic strain energy (Example I). (a) Kinetic energy versus time for various structural members. (b) Ratio of KE_{bm}/KE_{ws} versus time. (c) Plastic strain energy versus time for various structural members. (d) Ratio of PE_{bm}/PE_{ws} versus time.

4.4. Integration method

A general implicit dynamic integration method is employed to solve the nonlinear dynamic problem. In order to ensure the accuracy of the numerical solutions with this method, an automatic incremental scheme is adopted to calculate the length of each time increment through a half-step residual control. The half-step residual is the equilibrium residual error (out-of-balance forces) halfway through a time increment. The acceptable half-step residual tolerance is specified by the HAFTOL option in ABAQUS, which has the dimensions of force and is usually chosen by comparison with typical actual force values such as applied forces. In this study, it is taken as a near approximate of the maximum blast pressure applied to the structure. Such an action will lead to a highly accurate solution for the problem and includes the effect of plasticity. This automatic incremental scheme is especially effective for the case where a sudden blast event initiates a dynamic problem and when the structural response involves large amounts of energy being dissipated by plasticity effects. In such a case, minor increments will be required immediately after the sudden blast event, while at later time steps the response can be modeled with equivalent accuracy with larger time increments. Moreover in order to limit the range of each time steps in the numerical simulations, the minimum and maximum allowable time increments are taken as 1×10^{-7} and 0.01 s, respectively.

5. Verification of finite element models

The verification of the finite element models as mentioned above is carried out by implementing it into the analysis of a simply supported beam subjected to blast loadings tested by Seabold (1967) and a square slab, clamped and longitudinally restrained along all edges exposed to uniform lateral pressure as tested by Keenan (1969). The computed and experimental displacement-time histories at the mid-span for the beam and the center of the slab are compared in Fig. 9. It can be observed that for the simply supported beam a peak experimental response of 28.5 mm was recorded at 19.5 ms. This agrees well with the analytical results for which the computed peak displacement of 28.8 mm that was reached at 19.2 ms. The recorded permanent deformation of this beam was 20.8 mm. It also correlated well with the predicted deflection of 21.7 mm. In the case of the RC slab, the maximum deflection at the center recorded from the experiment was 12 mm that appeared at time 7.4 ms, which is fairly close to the numerically predicted deflection of 11.9 mm at time 7.2 ms. In addition, the analytical and experimental results of top compressive strain history of concrete, strain history of main reinforcement, support reaction history, and mid-span velocity history of the RC structural member are also compared in Fig. 9. It is demonstrated that the numerical analysis reasonably agrees with the observed experimental behaviors. Therefore the numerical model integrated into the nonlinear anal-

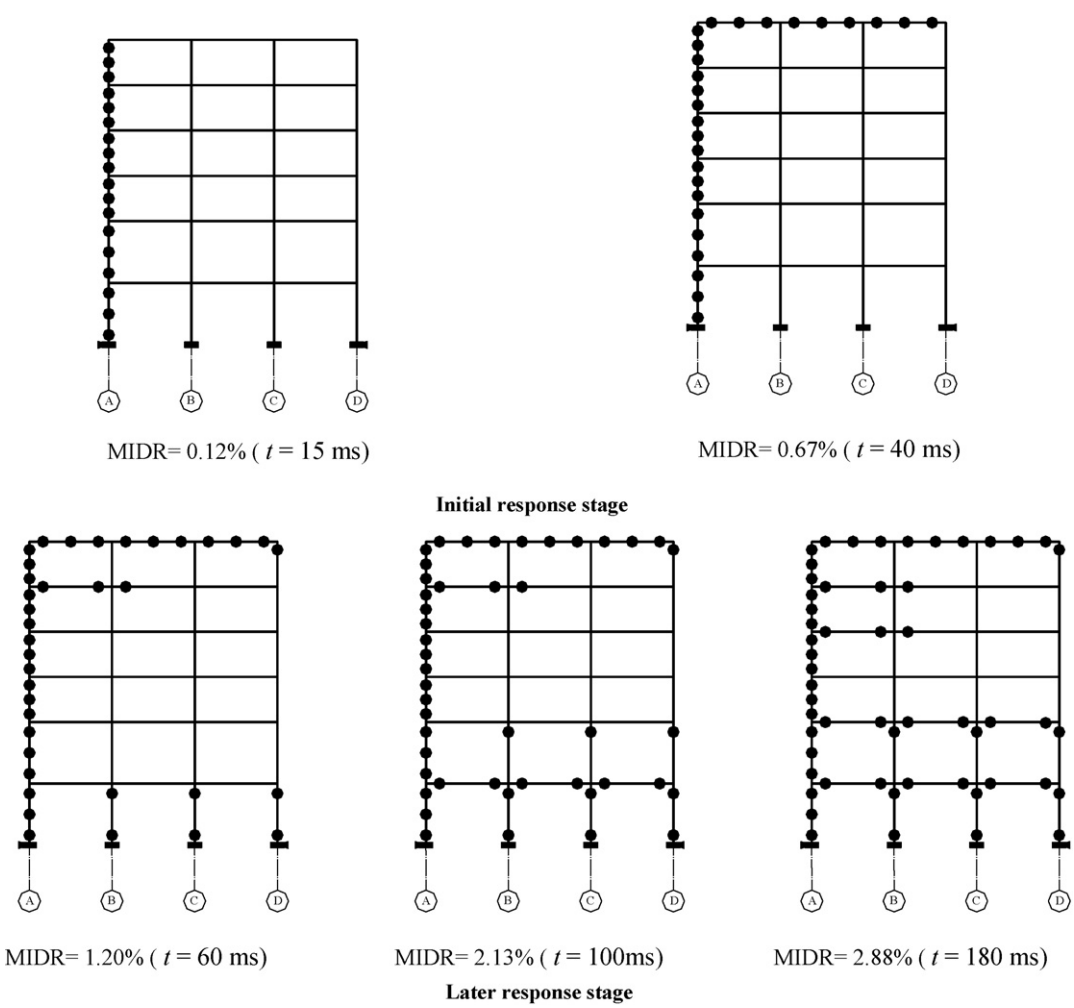

Fig. 11. Damage propagation with time (Example I).

ysis of the blast-loaded six-storey frame structure has shown to have the ability to simulate the failure process of concrete and reinforcement.

6. Numerical examples

6.1. Example I—frame structure with exterior cladding panels

In order to obtain a general view of the dynamic responses of the six-storey frame structure with RC exterior cladding panels under the considered blast condition, its energy responses including the kinetic energy and the plastic strain energy are plotted in Fig. 10. In these figures, the symbols of KE_{ws} and PE_{ws} are the kinetic energy and plastic strain energy within the whole structure respectively. KE_{bm} and PE_{bm} represent their respective energies within the critical blast-loaded members (including the front exterior cladding panels and columns, the top-storey beams and roof slabs) while KE_{om} and PE_{om} represent the kinetic and plastic strain energies within other structural members, respectively.

From Fig. 10, it can be observed that from 0 ms to 30 ms, KE_{bm} composes the most significant part of KE_{ws} covering averagely about 85%. This reflects the predominant role of the localized responses of the critical blast-loaded members in the structural responses during this time frame. Subsequently, the ratio of KE_{bm}/KE_{ws} decreases rapidly to a value of approximately 23% at about 50 ms and keeps almost constant at that value. This demonstrates that the dynamic response of the structure is in a mode where the global response of

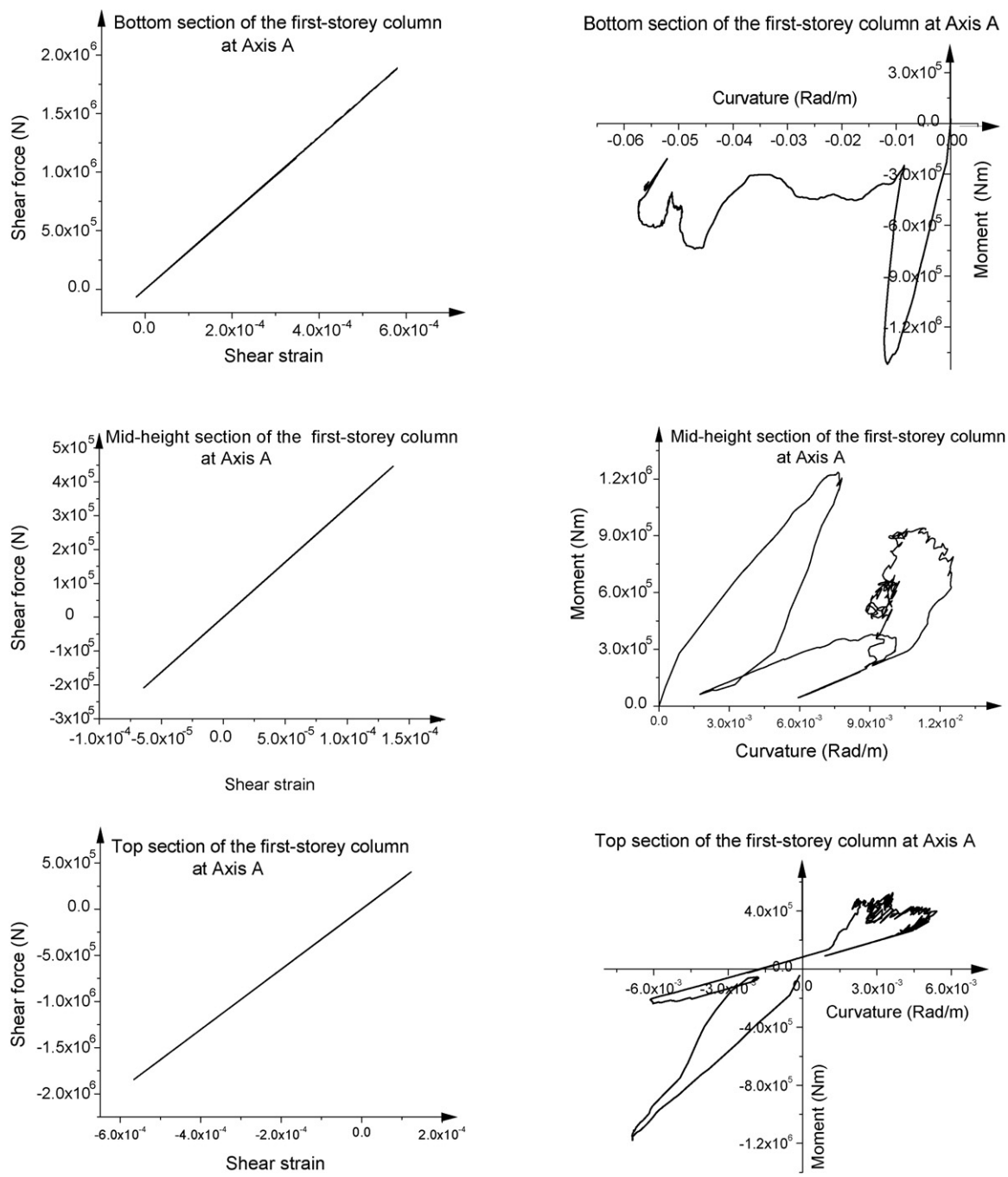

Fig. 12. Responses of the first-storey column at Axis A (Example I).

the structural system as a whole dominates. Therefore, the entire dynamic response of the structure can be approximately divided into two stages at a time of 40 ms as shown in Fig. 10(b). Within the initial stage, the dynamic responses are concentrated on several critical blast-loaded members while as time progresses, more structural members are motivated and the structural global responses become more predominant. The plastic strain energy response of the structure shows the same stage division as illustrated in Fig. 10(d) where the ratio of PE_{bm}/PE_{ws} versus time is plotted. PE_{bm} accounts for almost all of PE_{ws} at the time of 40 ms. However with the global response of the structure motivated later, more plastic deformation occurs on the members other than the critical blast-loaded ones and thus the ratio of PE_{bm}/PE_{ws} declines. A more detailed description of the structure responses and its damage propagation with time will be made in the following sections with reference to these two response stages.

6.1.1. Initial response stage

At the initial response stage, both kinetic and plastic strain energy responses are concentrated on critical blast-loaded members. As such, special attention is focused on their dynamic responses and corresponding damage levels with the respective plastic hinge distributions, as plotted in Fig. 11. A flexural plastic hinge is assumed to initiate when the longitudinal tensile reinforcement first yields at a point along the beam element and the hinge will continue to spread over a continuous portion of the beam. Thus the occurrence time of the hinge corresponds with the first appearance of plastic strain of reinforcement whose variation with time can be found from the numerical analysis in ABAQUS (2005).

It can be observed from Fig. 11 that due to the intensive localized responses on these members induced by the blast loadings during this stage, three plastic hinges have been formed on the bottom, mid-height and top sections of the front columns at 15 ms as well as the left end, mid-span and right end sections for the top-storey beams at 40 ms. This results in a typical damage mechanism similar to that on the flexural structural members. The difference between the time of forming this damage mechanism on the front columns and top-storey beams is caused by the difference of the time when the peak blast pressures acting upon them is attained. As for the other frame members (beams and columns), almost no plastic deformation is present.

The flexural deformation plays a relatively important role on the dynamic responses of structural members under distant blast conditions as indicated in Fig. 12, where typical moment-curvature and shear force–shear strain curves for different cross-sections of the first-storey columns at A–A are plotted. It can be seen that a linear relationships exist between the shear forces and the shear strains for these cross-sections while all the irrecoverable deformation is induced by their curvature responses. These phenomena are reflected on the cross-sectional responses of other structural members as well.

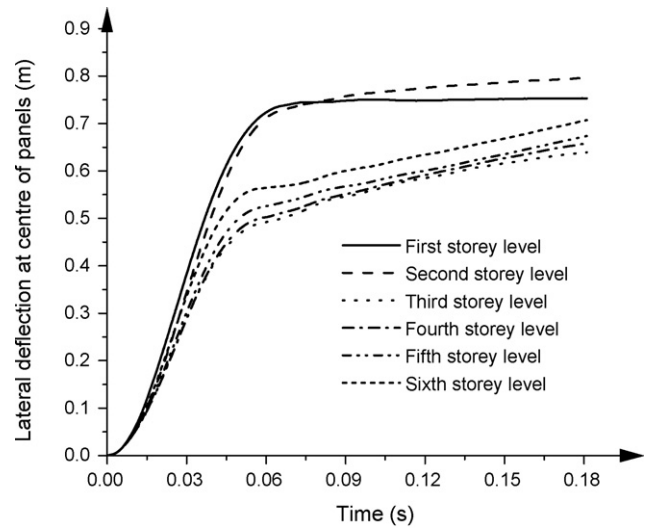

Fig. 13. Lateral deflection of the front cladding panels (Example I).

The responses of the front exterior cladding panels are significantly severe as illustrated in Fig. 13. This is due to the direct action of the blast loadings on them as well as their large dimensions that receive the blast loadings during the initial response stage. The lateral deformation at the center of the first-storey exterior cladding panel reached 653 mm at the end of the initial response stage. This is approximately equivalent to a support rotation of 16.5°. According to the actual resistance deflection function presented in TM5-1300 (1990), the resistance due to the tensile membrane action produced under the continuous reinforcement conditions as well as adequate lateral constraint, increases with increasing deflection up to incipient failure at approximately 12° support rotation. Based on this, the cladding panel is almost in a failure state by the end of the initial response stage.

Fig. 14 shows the storey lateral displacement (storey drift) responses for the global response of the structural system. It is indicated that all floor levels have the similar drifts (about 30 mm) at the time of 40 ms, except for the roof whose drift is somewhat smaller. This works out to provide a concentrated Maximum Inter-Storey

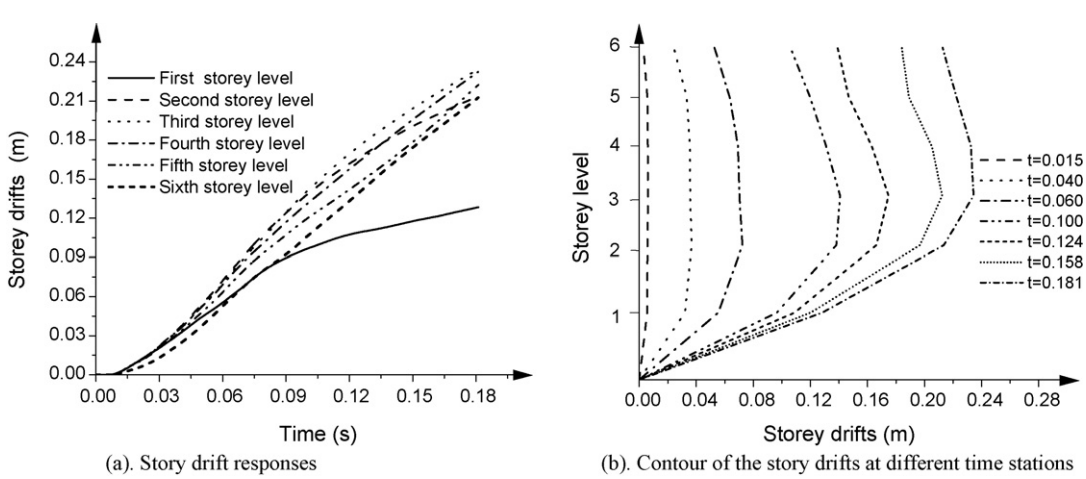

Fig. 14. Storey drifts for the structure (Example I). (a) Storey drift responses. (b) Contour of the storey drifts at different time stations.

Drift Ratio (MIDR—the drift difference between adjacent storeys), of about 0.67%. This is the ratio of maximum inter-storey drift to the inter-storey height occurring at the first storey. The contour of the storey drifts for the structure at this time location can be found in Fig. 14b.

6.1.2. Response stage II

At the later response stage II, the structural dynamic response moves to a mode where the global response of the structural system dominates as a whole. Hence, the distribution of damage as well as its propagation with the progression of time is in a different manner as compared to the initial response stage I. During this response stage, plastic hinges are formed firstly on both end sections of the first-storey columns at a time of about 60 ms as the inter-storey drift within this storey increases as shown in Fig. 11. Subsequently, the damage spreads upward with more plastic hinges successively forming on connected cross-sections around the joints located in the first and second floor levels. Since the plastic hinges formed at this stage are caused by large global sideway responses, they appear only at the end sections of structural members.

The storey drift distributions with time for this frame structure under the concerned blast condition are demonstrated in Fig. 14, to provide a better understanding of structural global responses. It can be seen that during the time of up to 80 ms the structural global responses are obviously concentrated within the first storey while the inter-storey drifts within other storey levels are trivial. As time progresses, the increase in the gradient of the first-storey drift drops to a relatively small value and the structural global response

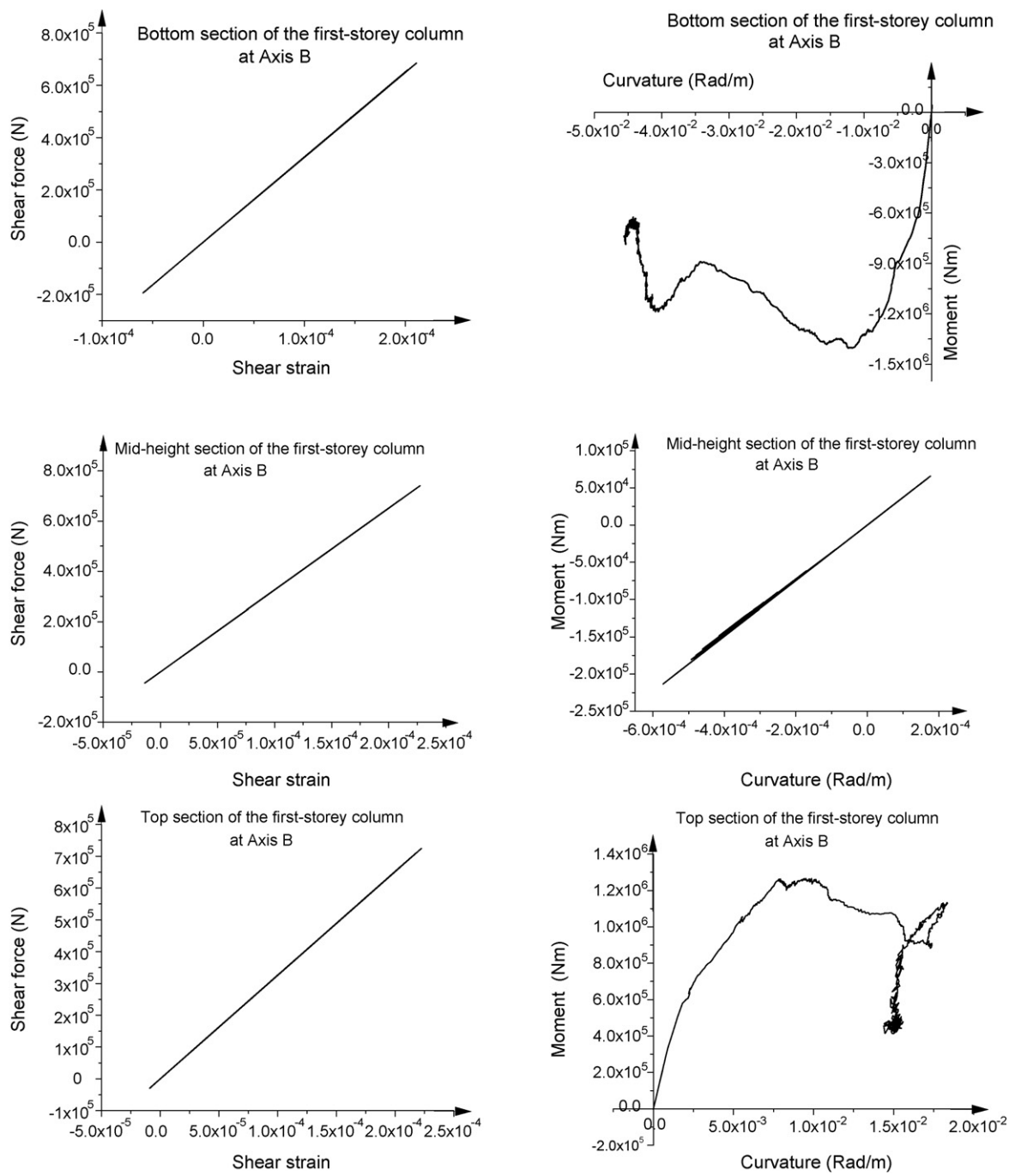

Fig. 15. Responses of some structural members other than blast-loaded ones (Example I).

Table 1
Three response levels.

Response level	Inter-storey drift ratio	Damage description
Low	1/50	Localized building/component damage
Medium	1/35	Widespread building/component damage
High	1/25	Building/component losing structural integrity and having possibility of collapse due to environment condition

begins to focus on the second-storey level. The structural maximum inter-storey drifts within the two critical storey levels (the first and the second storeys) have reached 129 and 85 mm, which are equivalent to a MIDR of 2.88% and 1.90% respectively by the time of 180 ms. Referring to Table 1, where a global damage criteria based on the inter-storey drift ratio for a frame structure under blast conditions have been suggested in the reference (Bounds, 1997), the frame structure at time 180 ms has sustained a high level of damage.

From the structural global responses concentrated in the first and second-storey levels at the time of 180 ms, it can be deduced that plastic rotations of the joints distributed in the first and second floor levels are focused on those cross-sections at the ends of the connected columns and beams as shown in Fig. 11. Typical moment-curvature and shear force–shear strain curves for these cross-sections where plastic hinges are formed at the later response stage II are plotted in Fig. 15. It is clear that plastic deformation is induced by their flexural responses where irrecoverable curvatures appear at the end sections of the members.

6.2. Example II—bare frame structure

The numerical simulation results of the energy responses for the six-storey bare frame structure under the concerned blast condition are presented in Fig. 16. It can be seen that due to the absence of the exterior cladding panels, a bare frame will experience a much slighter dynamic responses as compared with the previous case. Therefore much less damage is induced as shown in Fig. 16(b) where only a small magnitude of 1.0 kN m of plastic energy appears on the floor slabs. As for the frame members (columns and beams) there are no plastic deformations present on them.

The responses of structural storey drift plotted in Fig. 17a demonstrate that the maximum inter-storey drift, which happens at the second-storey level, is only about 9.5 mm and is the equivalent to a MIDR of 0.21%. The MIDR's within other storey levels are smaller than this value and thus there is no global damage to the structure under this blast condition (SEAOC, 1995). In addition, from the storey drift contours at different time stations shown in Fig. 17b, it is obvious that the maximum storey drift occurs initially at the first storey whereas with the progression of time it will move

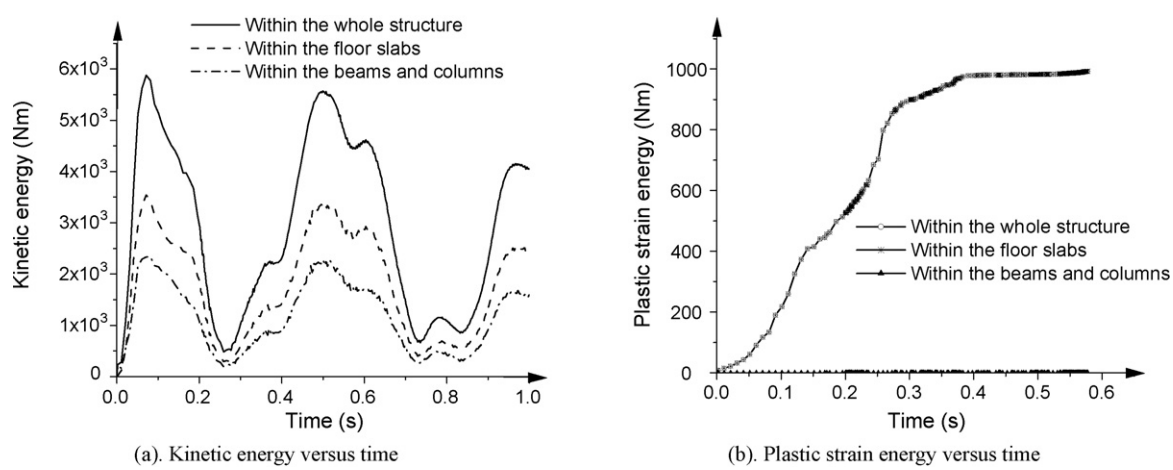

(a). Kinetic energy versus time (b). Plastic strain energy versus time

Fig. 16. Responses of the kinetic energy and plastic strain energy (Example II). (a) Kinetic energy versus time. (b) Plastic strain energy versus time.

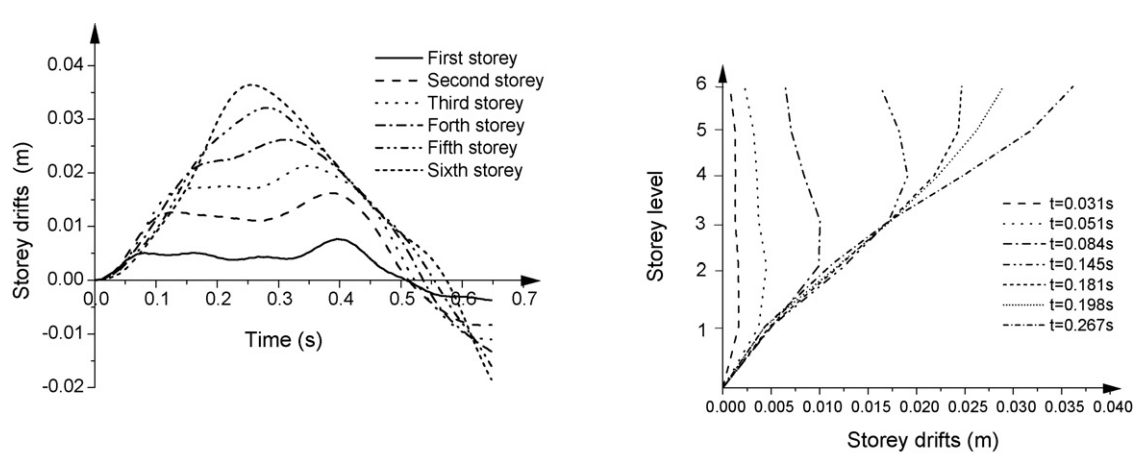

(a) Story drift responses (b) Contour of the story drifts at different time stations

Fig. 17. Storey drifts for the structure (Example II). (a) Storey drift responses. (b) Contour of the storey drifts at different time stations.

upward the structure in the sequence of the floors. Thus a transverse wave is formed in the frame structure.

7. Summary

The study presented in this paper investigates the responses of RC frame structures that are typical of turbine buildings located within nuclear power plants, with and without exterior cladding panels when exposed to distant intense surface explosions. The following conclusions may be drawn:

1. The study provides an insight into the behavior of typical turbine building frame structures when subjected to distant intense blast loadings. These blast scenarios are typical of accidents or intended attacks from terrorist organizations.
2. The response of the frame structures with RC exterior wall panels can be approximately divided into two stages. They are the localized responses of the blast-loaded members that are critical during the initial response of stage I, and the global responses of the structural system that dominate the later response of stage II. In addition, the flexural responses play a more important role in the plastic deformation of the beams and columns in the frame in comparison to their respective shear responses.
3. The existence of RC exterior cladding panels produces more severe dynamic responses than those of the bare frame structure with all other blast parameters held constant. Reflected pressure will quickly reduce to zero for the bare frame structure and only the drag forces associated with dynamic pressures are critical in the net blast loadings on the structure. This is due to the diffraction of the blast waves around the columns. However, the exterior cladding panels cause the structure to be loaded with reflected blast pressure, overpressure, and dynamic pressure, thus causing the blast forces subjected to the frame structure with cladding panels to be much greater. The numerical simulations show that some plastic deformation would appear to the structure to dissipate the work produced by such a large blast force, and results in the structure experiencing some levels of damage.
4. The results obtained emphasizes that the concept of using ductile exterior cladding as a mechanism for the control of blast response appears to be somewhat unorthodox. Its potential benefits warrant further investigation. It is apparent that if proper ductile panel response is utilized, the concept should be very effective for enhancing the blast resistant performance of turbine buildings within nuclear power plants and provide them with the much needed additional level of security.

References

ABAQUS, 2005. ABAQUS/Standard User's Manual. HKS, Inc.

ASCE Manual 42, 1985. Design of structures to resist nuclear weapons effects. American Society of Civil Engineers.

Baker, W.E., Cox, P.A., Westine, P.S., Kulesz, J.J., Strehlow, R.A., 1983. An Explosion Hazard and Evaluation: Fundamental Studies in Engineering. Elsevier Scientific Publishing Company, NY.

Biggs, J.M., 1964. Introduction to Structural Dynamic. McGraw-Hill, New York.

Bounds, W.L., 1997. Design of blast resistant building in petrochemical facilities, ASCE Task Committee Report on Blast Resistant Design.

BS 8110, 1997. Structural use of concrete: code of practice for design and construction. British Standard.

CEB-FIP Model Code 1990, 1993. Design code. Thomas Telford, Switzerland.

Corley, W.G., Mlakar, P.F., Sozen, M.A., Thornton, C.H., 1998. The Oklahoma City bombing: summary and recommendation for multi-hazard mitigation. Journal of Performance of Constructed Facilities, ASCE 12 (3), 100–112.

Dharan, C.K.H., Hauser, F.E., 1970. Determination of stress–strain characteristics at very high strain rates. Experimental Mechanics 10, 370–376.

Forbes, D.F., 1999. Blast loading on petrochemical buildings. Journal of Energy Engineering, ASCE 125 (3), 94–102.

Fu, H.C., Erki, M.A., Seckin, M., 1991. Review of effects of loading rate on concrete in compression. Journal of Structural Engineering, ASCE 117 (12), 3645–3659.

Georgin, J.F., Reynouard, J.M., Merabet, O., 1998. Modeling of concrete at high strain rate. Computational Modeling of Concrete Structures 2, 593–601.

Glasstone, S., Dolan, P.J., 1977. The Effects of nuclear Weapons, third ed. U.S. Dept. of Defense and U. S. Dept. of Energy, Washington, D.C.

Hilleborg, A., Modeer, M., Petersson, P.E., 1976. Analysis of crack formation and crack growth in concrete by means of fracture mechanics and finite elements. Cement and Concrete Research 6, 773–782.

Keenan, W.A., 1969. Strength and behavior of restrained reinforced concrete slabs under static and dynamic loadings, Technical Report R-621, Y-F008-08-02-123, DASA-RSS3318, Naval Civil Engineering Laboratory, California.

Kletz, T.A., 1975. The Flixborough Cyclohexane Disaster, vol. 8. Loss Prevention, American Institute of Chemical Engineers, New York, pp. 106–118.

Longinow, A., Mniszewski, K.R., 1996. Protective building against vehicle bomb attacks. Practice Periodical on Structural Design and Construction, ASCE 1 (1), 51–54.

Luccioni, B.M., Ambrosini, R.D., Danesi, R.F., 2003. Analysis of building collapse under blast loads. Engineering Structures 26 (1), 63–71.

Malvar, L.J., Crawford, J.E., 1998a. Dynamic increase factors for concrete. In: Twenty-Eighth DDESB Seminar, Orlando, FL.

Malvar, L.J., Crawford, J.E., 1998b. Dynamic increase factors for steel reinforcing bar. In: Twenty-Eighth DDESB Seminar, Orlando, FL.

Seabold, R.H., 1967. Dynamic Shear Strength of Reinforced Concrete Beams, Part II. Naval Civil Engineering Laboratory, Port Hueneme, California.

SEAOC, 1995. Performance based on seismic engineering of buildings. The Structural Engineers Association of California, San Francisco, USA.

Smith, P.D., Hetherington, J.G., 1994. Blast and Ballistic Loading of Structures. Butterworth-Herinmann Ltd., Linacre House, Jordan Hill, Oxford.

TM 5-855-1, 1986. Fundamental of protective design for conventional weapons. United States Department of the Army, Washington, D.C.

TM5-1300, 1990. Structures to resist the effects of accidental explosions. United States Department of the Army, Washington, D.C.

Bing Li is an Associate Professor in the School of Civil and Environmental Engineering at Nanyang Technological University, Singapore.

Tso-Chien Pan is a Professor in the School of Civil and Environmental Engineering at Nanyang Technological University, Singapore.

Anand Nair is a MEng candidate in the School of Civil and Environmental Engineering at Nanyang Technological University, Singapore. He received his B.Eng.(Hons) from the Nanyang Technological University, Singapore.